Measurements of impulsive reconnection driven by nonlinear Hall dynamics

T. D. Tharp,[1] A. F. Almagri,[1] M. C. Miller,[1] V. V. Mirnov,[1] S. C. Prager,[1] J. S. Sarff,[1] and C. C. Kim[2]
[1]*University of Wisconsin-Madison, 1150 University Ave., Madison, Wisconsin 53706, USA*
[2]*University of Washington, Seattle, Washington 98105, USA*

(Received 5 August 2010; accepted 8 November 2010; published online 10 December 2010)

The magnetic fields associated with reconnection in the edge of the reversed field pinch configuration have been measured in the Madison Symmetric Torus. The measured magnetic field structure is compared with theoretical predictions computed in both toroidal and cylindrical geometries. The summation of multiple modes has been accomplished to reveal a complex but still coherent edge structure. Key terms of relevant Ohm's law are accessible from magnetic field measurement and reveal the ordering $[(1/ne)J\times B \gg E > \eta J]$, which implies that two fluid effects are important in the physics governing this reconnection. Further, it is seen that the nonlinear three-wave coupling of the Hall term acts as a driving mechanism for this linearly stable mode. © *2010 American Institute of Physics*. [doi:10.1063/1.3521336]

Magnetic reconnection—the often violent process by which magnetic fields are topologically rearranged into a new magnetic geometry—has been identified in a variety of astrophysical and laboratory plasmas.[1] Sweet[2] and Parker[3] offered the first quantitative description of this process to explain astrophysical observations. Subsequently, many theoretical variations have been proposed to describe reconnection more accurately, particularly focusing on the explanation of fast and impulsive reconnection. Models which treat the electron fluid and ion fluid independently allow for the inclusion of the Hall term in the applicable Ohm's law and are a particularly promising way to explain the observed rates of fast reconnection.[4] Models which result in impulsive reconnection typically invoke nonlinear or three-dimensional effects.[5]

Reconnection appears in nature and in laboratory plasmas in two general forms: driven and spontaneous. Driven reconnection occurs only because of external forcing, whereas spontaneous reconnection results from the development of a local instability which allows the plasma to reach a lower energy state.[6] A classic form of spontaneous reconnection, known as a tearing instability, will occur in a toroidal plasma when two conditions are met. First, if the geometry permits a quantized wave vector with no parallel component ($\vec{k}\cdot\vec{B}=0$), the mode will be resonant. Second, depending on the details of the plasma equilibrium, the mode may also be unstable.[7] In particular, instability can be induced by a strong gradient in the plasma current density such that the associated gradient length scale is shorter than k^{-1}.[6]

The reversed field pinch (RFP) (Ref. 8) is a toroidal plasma configuration with strong shear in the mean (equilibrium) magnetic field. The RFP typically displays a periodic sawtooth cycle characterized by a slow peaking of the current profile followed by a sudden global relaxation event that relaxes gradients. During these events, magnetic tearing reconnection occurs at multiple radial locations where different Fourier modes are resonant. Modes resonant in the core region appear spontaneously through linear instability associated with the gradient in the current profile. Modes resonant in the edge region are predicted and measured to be linearly stable, but are inferred to grow to large amplitude through nonlinear drive.[9,10] While the resonant surfaces are localized due to the strong magnetic shear, the core-resonant and edge-resonant modes have global radial structure, allowing them to interact nonlinearly.

In this letter we report detailed magnetic field measurements of the driven reconnection associated with the dominant Fourier mode in the edge of an RFP. We compare the large-scale radial structure of the reconnection magnetic field with a magnetohydrodynamic (MHD) prediction in toroidal geometry and find excellent agreement. Although the large-scale radial structure agrees with MHD, the dynamics of the reconnection layer and drive do not. We measure the terms in Ohm's law which are accessible through an assortment of magnetic diagnostics. We find that the Hall term is large compared to both the electric field and the resistive term $[(1/ne)J\times B \gg E > \eta J]$, indicating that two fluid effects are important for the magnetic reconnection of this edge-resonant mode. The observed Hall term is large at the spatial location of the reconnection X-point, a result which is somewhat different from the traditional picture of Hall reconnection. The strongest contributions to the measured Hall term arise from nonlinear three-wave coupling to the linearly unstable modes resonant in the core. Thus, unstable magnetic reconnection sites resonant in a far region of the plasma can provide the external forcing to drive the local reconnection of a mode that would be stable in isolation and the nonlinear interaction is mediated by the Hall term of the generalized Ohm's law.

These measurements were performed on the Madison Symmetric Torus (MST),[11] an RFP with major radius $R=1.5$ m and minor radius $a=0.52$ m, using insertable magnetic probes in standard 225 kA plasmas. Measurements are taken near the resonant surface of the dominant edge-resonant mode, which is located where the toroidal component of the mean field vanishes ($B_\phi=0$). Radial profiles of

the magnetic fluctuations within the plasma are constructed from the correlation of insertable probe data with data from a toroidal array of 64 magnetic pick-up coils on the inner wall of MST. Correlation analysis allows us to extract the spatial Fourier mode structure of a single-point measurement within the plasma. The Fourier decomposition of the magnetic field at the plasma boundary ($r=a$) is measured by the toroidal array. These measurements as well as the local insertable probe measurement are recorded for many realizations of the sawtooth reconnecting plasma. Averaging over this ensemble of realizations in a particular manner extracts the toroidal mode number decomposition (n-spectrum) associated with the single-point probe measurement. Repetition of this process with the probe inserted to different radial positions results in the toroidal magnetic field spectrum as a function of radius.

All signals are Fourier decomposed into

$$S(\theta,\phi)=\sum_{m,n} s_{m,n}e^{i(m\theta+n\phi)}.$$

Each n mode has a dominant m component ($m=0$ for $n\leq 4$; $m=1$ for $n\geq 5$), so we approximate $m=m_n$, and

$$S(\theta,\phi)=\sum_{n} s_{n}e^{i(m_n\theta+n\phi)}.$$

To extract the spectrum of a probe signal, S, we assume *a priori* that S is strongly coupled to the magnetic field at the wall such that

$$s_n(r,t)e^{i(m\theta+n\phi)}=c_n(r,t)x_n(a,t)e^{i(m\theta+n\phi)},$$

where c_n is a complex constant of proportionality and is the same for every realization of the sawtooth and $x_n(a,t)$ represents the amplitude and phase of the magnetic field measured at the wall. The quantity s_n may in general have a random phase, but the averaging method described below identifies a statistically constant phase relative to x_n. The quantity of interest is then $\mathbf{s}_n=|s_n|e^{i(\delta_{xn}-\delta_{sn})}=c_n|x_n|$. This approach is very reasonable for magnetic field since magnetic structures are radially broad in MST plasmas.

It is seen experimentally that during each sawtooth realization a given magnetic mode develops in the plasma at a different random phase. In this case, there is an approximate equivalence between an ensemble average of many similar sawtooth events and an average over toroidal angle of a single typical event. This provides the context for a more intuitive discussion in which average quantities in the spatial domain are calculated, with the understanding that we will substitute an ensemble average for a toroidal average whenever data is processed.

It can be shown[12] that

$$\mathbf{s}_n=\frac{2\langle SX_n\rangle-2i\langle SX_n^{\dagger}\rangle}{\langle|x_n|\rangle}, \tag{1}$$

where $\langle\cdots\rangle$ indicates an average (over toroidal angle or sawtooth ensemble), $S(r,t)$ is the probe signal within the plasma, and $X_n^{[\dagger]}(a,t)$ is the value of the [90° phase shifted] magnetic field of the (m,n) toroidal mode, measured at the wall by the toroidal array and evaluated at the angular (θ and ϕ) location of the probe. A measure of confidence can be found by calculating an autocorrelation using a single toroidal array coil (i.e., using one coil of the toroidal array as the "probe"). This check shows that Eq. (1) correctly reproduces the average mode amplitude and phase for modes $n=1-8$ for a typical ensemble of about 200 similar sawteeth. One standard deviation in ensemble statistics is used to calculate the error associated with all measurements presented.

In Figs. 1(a)–1(c), this method has been used to measure the magnetic field associated with the $n=1$ mode. This mode is predominately $m=0$ but has harmonic content arising from the toroidal geometry. The best theoretical context for future comparison will be full 3D, nonlinear, two fluid computation, which is only now becoming possible with state-of-the-art codes. Presently, measurements are compared with eigenfunctions calculated in cylindrical geometry using a linear resistive MHD eigenvalue code[13] and with profiles calculated in a toroidal geometry from linear initial-value single-fluid simulations using NIMROD.[14] Though this mode is nonlinearly driven in the experiment, the comparison with linear theory is justified by noting that slowly varying magnetic perturbations have robust global spatial structures. Since the timescales of the sawtooth cycle are much longer than the Alfvenic timescale, the magnetic profiles are weakly sensitive to the mechanism—linear or nonlinear—of the mode excitation.[15]

Both of these linear calculations (cylindrical and toroidal) require evaluation of an equilibrium which is unstable to the $n=1$ mode. It has been shown recently[16] that there is a wide class of equilibrium current profiles for which the $m=0$ mode is spontaneously unstable, some of which are very close (in terms of global parameters) to the experimentally realized equilibrium. One of these profiles, which supports an unstable $m=0$ mode but has an equilibrium close to that of the experiment, was chosen for evaluation and used for both cylindrical and toroidal calculations. The comparison shown in Figs. 1(a)–1(c) illustrates substantial differences between the cylindrical and toroidal computations and shows strong agreement between experimental profiles and toroidal computation.

Figures 1(d)–1(f) show the measured B_θ and B_ϕ mode amplitude profiles for $n=6-8$, respectively. While toroidal effects could play a role in the structure of these modes, toroidal calculations are not yet available for comparison. We include the measured profiles here for reference in our later discussion of Hall term measurements.

With measurement of the mode-resolved magnetic field in hand, the reconnection field structure can be visualized by plotting contours of toroidal flux. Integration of the measured toroidal field from the wall using only the equilibrium field and the $n=1$ component results in the toroidal flux associated with the $n=1$ reconnection. Contours of this flux yield a visualization of the associated two-dimensional field lines, shown in Fig. 2(a). The addition of the mode contributions from $n=2$, 3, and 4, including the relative phases of these modes, provide a more complete visualization of the magnetic field, seen in Fig. 2(b). In particular, the addition of these modes does not destroy the overall shape of the $n=1$ island, indicating that a coherent $m=0$ dominated structure

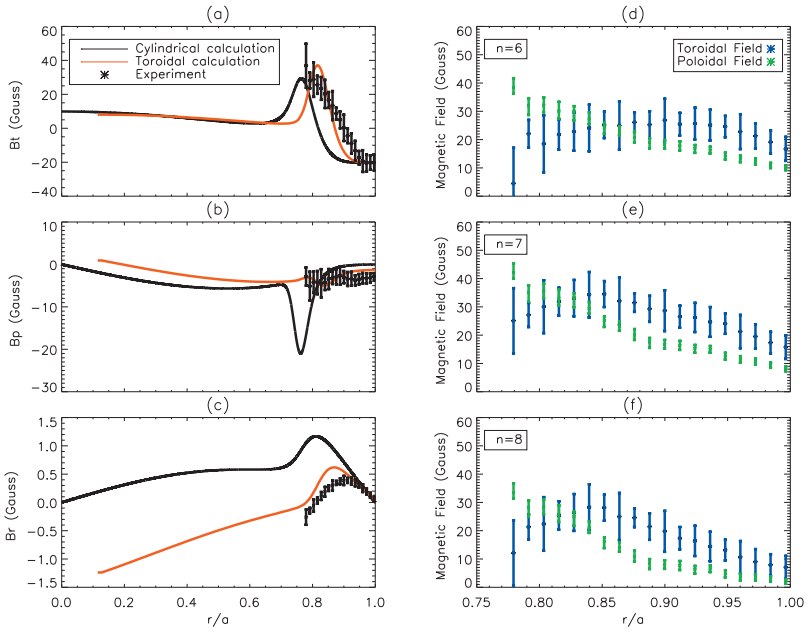

FIG. 1. (Color) Panels (a), (b), and (c) show the dominant part (real or imaginary) of magnetic field profiles for $n=1$ B_ϕ, B_θ, and B_r, respectively; for cylindrical calculation (black), toroidal calculation (red), and data (points). Since the complimentary part (imaginary or real) is small, these can be interpreted as the mode's amplitude with relative sign information included. The experiment's radial magnetic field, B_r, is inferred from $\nabla\cdot\vec{B}=0$. Measurements of B_r are consistent with the inferred values but have much larger error bars. Panels (d), (e), and (f) show the B_θ (green) and B_ϕ (blue) measured profiles for $n=6$, 7, and 8, respectively.

likely exists in these plasmas. The addition of mode content $n>4$ would be yet more complete, but these modes have dominant $m=1$ and therefore a different direction of symmetry that cannot be visualized on the same two-dimensional toroidal flux plot.

To identify the driving mechanism for $n=1$ reconnection, we examine generalized Ohm's law

$$E+v\times B-\eta J-\frac{1}{ne}J\times B+\frac{1}{ne}\nabla\cdot P-\frac{m_e}{ne^2}\frac{\partial J}{\partial t}=0 \qquad (2)$$

evaluated for this mode by applying the mathematics of Eq. (1) to the entirety of Eq. (2). Again, it is conceptually advantageous to consider the average as a spatial average over toroidal angle ϕ.

The analysis of magnetic probe measurements results in the Fourier spatial structure of the field ($\tilde{B}=B_n=|b_n|e^{i(n\phi+m\theta-\delta)}$) as a function of radius; therefore, all spatial derivatives of $\tilde{B}$ are known. Four terms of the parallel Ohm's law (θ direction) can be evaluated for $m=0$ modes from magnetic field measurements. (1) The parallel electric field, $\tilde{E}_\theta$, has no electrostatic component ($\nabla_\theta\Phi=0$ for $m=0$ modes), so Faraday's law gives $E_\theta=-(iR/n)(\partial B_r/\partial t)$. (2) Current density is evaluated from Ampere's law, $\tilde{J}=\nabla\times\tilde{B}$. The resistive term is evaluated using local Langmuir probe measurements of temperature and density to calculate the Spitzer resistivity, using $T_e=60$ eV, $n_e=10^{19}$ m^{-3}, $Z_{\text{eff}}=3$. (3) The Hall term can be evaluated mode-by-mode, $(J\times B)_n=(J_0\times B_n)+(J_n\times B_0)+$nonlinear terms. Nonlinear Hall terms will be discussed in detail below. (4) The electron inertia term, $(m_e/ne^2)(\partial J/\partial t)$, has been calculated but is found to be negligibly small. We will not consider it further.

At each radius, the $n=1$ Hall term, $(J\times B)_{(n=1)}$, can be calculated from the independent Fourier decomposition of J and B. To illustrate, consider the nonlinear three-wave coupling of $n=6$ and 7 to $n=1$,

$$J_6(r)\times B_7(r)=|j_6|\cos(\theta+6\phi-\delta_{j6})\times|b_7|\cos(\theta+7\phi-\delta_{b7})$$
$$=\frac{|j_6||b_7|}{2}\gamma\cos(\phi+\delta_{J6}-\delta_{B7})+(n=13\ \text{wave}),$$

where γ is introduced to account for the statistical phase

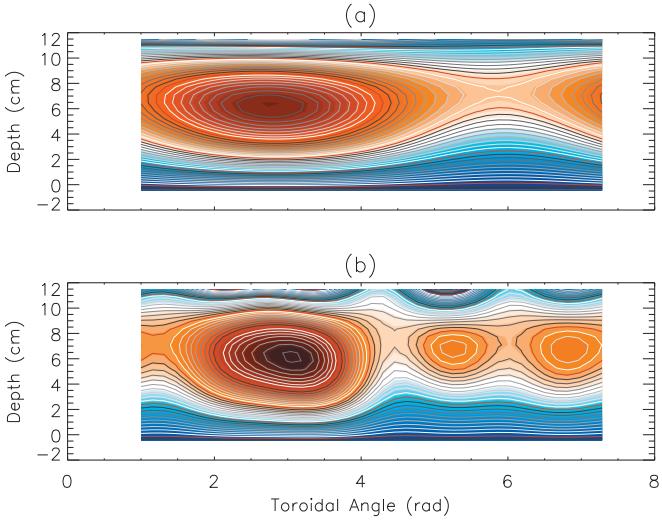

FIG. 2. (Color) Contours of toroidal flux in the reconnection ($r-\phi$) plane. (a) $n=1$. (b) $n=1-4$. Inclusion of $n=2-4$ compresses the O-point and damages the structure of the X-point. The conducting wall of MST is located along the bottom edge of the figure (depth=0).

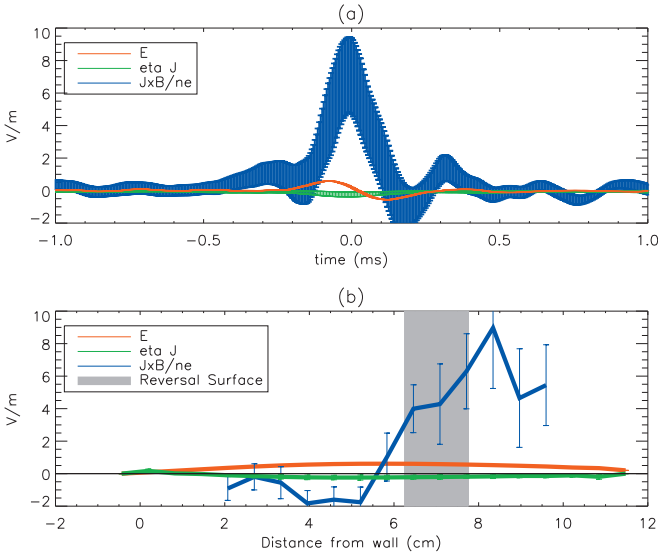

FIG. 3. (Color) Poloidal (parallel) Ohm's law terms for the $n=1$ mode as a function of (a) time and (b) radius. (a) Ohm's law terms vs time, evaluated at $r/a=.865$ (7 cm from the wall) and the phase (toroidal angle) associated with the X-point of $n=1$ reconnection. (b) Ohm's law evaluated at $t=-0.075$ ms, the approximate time of peak electric field.

alignment of the three modes. To calculate γ explicitly, we take the spatial variation of each mode pairing and substitute into Eq. (1) to find

$$(\tilde{J}_p \times \tilde{B}_q)_n = \frac{\mathbf{j}_p^*(r)\mathbf{b}_q(r)\langle|x_n||x_p||x_q|(e^{i(\delta_{x_n}+\delta_{x_p}-\delta_{x_q})})\rangle}{2\langle|x_n|\rangle\langle|x_p|\rangle\langle|x_q|\rangle},$$

with $q-p=n$. Here $|x_n|$ represents the amplitude of the nth mode, as measured by the toroidal array at the wall. While $\mathbf{j}_p^*(r)$ and $\mathbf{b}_q(r)$ are measured inside the plasma, the factor

$$\gamma = \frac{\langle|x_n||x_p||x_q|(e^{i(\delta_{x_n}+\delta_{x_p}-\delta_{x_q})})\rangle}{\langle|x_n|\rangle\langle|x_p|\rangle\langle|x_q|\rangle}$$

for this three-wave interaction is measured at the wall. This is called the bicoherence[17] of the three waves and represents the statistical phase alignment of the three modes. The amplitude of this quantity (ranging from 0 to 1) measures the degree of nonlinear coupling in the system. For these measurements, $|\gamma|\approx 0.9$ at the peak of the sawtooth, indicating the plasma is in a strongly nonlinear regime, and generally validating the analysis' assumption of strong coupling. The measured nonlinear Hall term presented is a sum over all three-wave terms of this type (i.e., sum over p and q, also including analogous terms with $p-q=n$) available for the evaluated modes, $n=0-8$. Correctly evaluating the phase of all modes allows Ohm's law terms to be evaluated at the toroidal location of the mode's X-point.

Figures 3(a) and 3(b) show the values of the measured $n=1$ X-point Ohm's law terms versus time and radius, respectively, using the sign convention $E=\eta J+(1/ne)J\times B+$(unmeasured terms). Without measurement of the remaining terms, experimental verification of the balance of Ohm's law is not available; however, we draw significant physics conclusions about the nature of this reconnection from the available measurements.

The measured ordering, $J\times B \gg E > \eta J$, implies that two fluid effects are an important contributor to the dynamics of this reconnection.[18] Island growth and decay are associated with positive and negative electric field, respectively, which may be taken as a measurement of the reconnection rate. The positive sign of the nonlinear Hall term at this location therefore indicates that it is driving term for reconnection during the first half of the sawtooth. Though it is not shown in these plots, it is observed that the linear Hall term, $(J_0\times B_n)+(J_n\times B_0)$, is small (less than 0.5 V/m) at this location and that the nonlinear Hall term is dominated by the contributions from the (1,6) and (1,7) coupling and the (1,7) and (1,8) coupling, indicating that it is the nonlinear coupling of these unstable core modes which provides the nonlinear Hall drive. The peaking of the Hall term in Fig. 3(b) can be traced back to the peaking of the toroidal field components of Figs. 1(d)–1(f).

Ohm's law observations are also supported by nonlinear simulation. In linear single-fluid tearing mode theory, the reconnection electric field is balanced by ηJ; in single-fluid nonlinear calculation using the nonlinear MHD code DEBS,[19] we have observed large positive nonlinear $-v\times B$ contributions in direct analogy to the nonlinear Hall term seen in the experiment.

In conclusion, we have measured the magnetic field structure of a driven edge mode in the RFP, which compares favorably with toroidal simulation, and deduced that the nonlinear Hall term of Ohm's law is a driving term for this mode. The broader impact of this result is that we have measured reconnection with the property that $E\neq\eta J$ at the $n=1$ reconnection X-point and that the nonlinear Hall term is capable of driving this reconnection.

[1] M. Yamada, R. Kulsrud, and H. Ji, Rev. Mod. Phys. **82**, 603 (2010).
[2] P. A. Sweet, *Proceedings from International Astronomical Union Symposium*, Stockholm, 1956, edited by B. Lehnert (Cambridge University Press, New York, 1958), Vol. 6, p.123.
[3] E. N. Parker, J. Geophys. Res. **62**, 509 (1957).
[4] J. Birn and M. Hesse, J. Geophys. Res. **106**, 3737 (2001).
[5] A. Bhattacharjee, Annu. Rev. Astron. Astrophys. **42**, 365 (2004).
[6] E. G. Zweibel and M. Yamada, Annu. Rev. Astron. Astrophys. **47**, 291 (2009).
[7] H. Furth, J. Killeen, and M. Rosenbluth, Phys. Fluids **6**, 459 (1963).
[8] H. A. B. Bodin and A. A. Newton, Nucl. Fusion **20**, 1255 (1980).
[9] Y. L. Ho and G. G. Craddock, Phys. Fluids B **3**, 721 (1991).
[10] S.-H. Choi, D. Craig, F. Ebrahimi, and S. C. Prager, Phys. Rev. Lett. **96**, 145004 (2006).
[11] R. N. Dexter, D. W. Kerst, T. W. Lovell, and S. C. Prager, Fusion Technol. **19**, 131 (1991).
[12] T. D. Tharp, Ph.D. thesis, University of Wisconsin-Madison, 2010.
[13] V. A. Svidzinski, G. Fiksel, V. V. Mirnov, and S. C. Prager, Phys. Plasmas **15**, 062511 (2008).
[14] C. R. Sovinec, A. H. Glasser, T. A. Gianakon, D. C. Barnes, R. A. Nebel, S. E. Kruger, D. D. Schnack, S. J. Plimpton, A. Tarditi, M. S. Chu, and the NIMROD Team, J. Comput. Phys. **195**, 355 (2004).
[15] P. Zanca and D. Terranova, Plasma Phys. Controlled Fusion **46**, 1115 (2004).
[16] V. Mirnov, C. Hegna, S. Prager, C. Sovinec, and H. Tian, Proceedings of the 21st IAEA Fusion Energy Conference, Chengdu, 2006.
[17] Y. C. Kim and E. J. Powers, IEEE Trans. Plasma Sci. **PS-7**, 120 (1979).
[18] C. Cothran, M. Landreman, and M. Brown, Geophys. Res. Lett. **32**, L3105 (2005).
[19] D. D. Schnack, D. Barnes, Z. Mikic, D. S. Harned, E. J. Caramana, and R. A. Nebel, Comput. Phys. Commun. **43**, 17 (1986).